Size-dependent photoluminescence in silicon nanostructures: quantum confinement effect

V. Kumar, K. Saxena, A.K. Shukla

Laser Assisted Materials Processing and Raman Spectroscopy Laboratory, Department of Physics, Indian Institute of Technology Delhi, New Delhi 110016, India
E-mail: akshukla@physics.iitd.ernet.in

Published in Micro & Nano Letters; Received on 28th November 2012; Revised on 18th April 2013; Accepted on 26th April 2013

Visible photoluminescence (PL) from laser-etched silicon nanostructures has been analysed. A systematic size dependence study of PL from silicon nanostructures has been performed. The PL from these structures is attributed to the quantum confinement effect. Different quantum confinement models have been used for PL and Raman lineshape fitting to calculate the mean size and size distribution of silicon nanostructures and the results are comparatively studied. Calculated values of oscillator strength and radiative lifetime show that PL is due to radiative recombination of confined excitons.

1. Introduction: Photoluminescence (PL) from silicon nanostructures (Si NSs) has stimulated enormous interest because of its potential applications in optoelectronics and biomedical/biophotonics [1, 2]. Crystalline silicon (c-Si) has been considered unsuitable for optoelectronic applications owing to its indirect electronic bandgap, which limits its efficiency as a light emitter. Light emission in indirect materials is naturally a phonon-assisted process with low probability since spontaneous recombination lifetimes are in the millisecond range [3]. Non-radiative recombination rates are much higher than that of radiative ones in c-Si and most of the excited electron–hole pairs recombine non-radiatively at room temperature. This results in very low internal quantum efficiency [4] of Si luminescence.

Room-temperature light emission has been observed in silicon when it is in the form of a low-dimensional system [5–9]. Low-dimensional silicon systems such as porous silicon [5, 6], silicon nanocrystals [7], silicon/insulator superlattices [8] and silicon nanopillars [9] etc. are being actively investigated as a means of improving light-emission properties. Many experimental efforts have been made to understand the nature of microstructures and the mechanism of PL in porous silicon [10–14]. The origin of PL from these NSs is discussed because of size and also because of oxide-related interfacial defect states [12] and surface states [14]. A complete understanding of the origin and mechanism of PL has not yet been achieved since the quantum confinement and surface effects are widely accepted in interpretation of PL [10–14]. Ding *et al.* [13] and Estes and Moddel [14] have proposed quantum confinement effect along with localised surface states for PL of Si NSs and have obtained different analytical expressions for PL spectra. Here, we are using a different analytical expression solely incorporating the quantum confinement effect to explain our experimental PL from Si NSs. Area under the PL spectrum is utilised here to calculate the oscillator strength of radiative transition for a given size of Si NSs.

In the work reported in this Letter article, Si NSs have been prepared by laser-induced etching (LIE) technique to neglect matrix effects on NSs. Optical phonon Raman spectra are used here to calculate the mean size and size distribution of Si NSs using theoretical Raman line shape fitting. A quantum confinement model has been used here to fit the PL spectra. The Si NSs fabricated on a clean surface, show visible PL at room temperature because of the quantum confinement effect. This is supported by the calculation of radiative lifetime using PL spectrum.

2. Experimental: Three samples (samples S1, S2 and S3) of Si NSs were fabricated by the LIE method [15]. Commercially available n-type Si (100) (resistivity ~5 Ω-cm) wafers were used for laser etching. Different samples S1, S2 and S3 were prepared by irradiating the wafers for 25, 45 and 60 min, respectively. The Raman and PL spectra were recorded using a spectroscopic setup of the triple monochromator (T64000 Jobin Horiba). Samples were excited with a photon energy of 2.41 eV from an argon-ion laser (COHERENT, INNOVA 90-5).

3. Results and discussion: Optical phonon Raman spectra are used here to calculate the mean size and size distribution using theoretical Raman line shape fitting of Si NSs. In Si NSs the selection rule $\Delta \boldsymbol{k} = 0$ of first-order Raman scattering (i.e. $\Delta \boldsymbol{k} = \boldsymbol{k}_f - \boldsymbol{k}_i$, where $\boldsymbol{k}_f$ and $\boldsymbol{k}_i$ are momentum vectors in final and initial vibrational levels, respectively) is relaxed [16, 17]. Therefore optical phonons away from zone-centre ($\Delta \boldsymbol{k} \neq 0$) also take part in the scattering process. For Si NSs, the optical phonons originating from the optical branch of phonon dispersion with ($\Delta \boldsymbol{k} \neq 0$) contribute to the Raman mode. Therefore first-order Raman intensity [18] for Si NSs is given by

$$I'(\omega) \propto \int_{L_1}^{L_2} N(L) \left[\int_0^1 \frac{\exp\left(-k^2 L^2/4a^2\right)}{\left[(\omega - \omega(k))^2 + (\Gamma/2)^2\right]} d^n k \right] \mathrm{d}L \qquad (1)$$

where '$N(L)$' is a Gaussian function of the form $N(L) \cong [\exp\{-(L - L_0)/\sigma\}^2]$ included to account for the size distribution of the NSs. L_0 is the most probable or average size of Si NSs and σ defines the width of distribution. L_1 and L_2 are the minimum and maximum size distribution of Si NSs, respectively. 'a' is the lattice parameter of c-Si and $\omega^2(k) = A + B\cos(\pi k/2)$ (where $A = 171\,400$ cm^{-2} and $B = 100\,000$ cm^{-2}) is the phonon dispersion curve for the optical branch of c-Si. Γ_o is the natural line width of the Raman mode of c-Si and 'n' shows the degree of confinement.

Figs. 1(*i*) (a–c) show the Raman spectra of samples S1–S3, respectively. The Raman spectra of these samples display the usual optical mode (i.e. 520.5 cm^{-1} for c-Si) that is shifted to a lower wavenumber with lineshape broadening and asymmetry towards the lower wavenumber. Phonon softening, full-width half maximum and the asymmetry of the optical mode are found to increase from samples S1 to S3. The Raman spectra of samples S1–S3 are theoretically fitted using (1) to calculate the average size of Si NSs. The theoretically calculated Raman line shape of these samples is shown by a solid line in Fig. 1(*i*). The best fit is obtained using $n = 2$. The sizes calculated by fitting Raman scattering data from samples S1, S2 and S3 using (1) are given in Table 1.

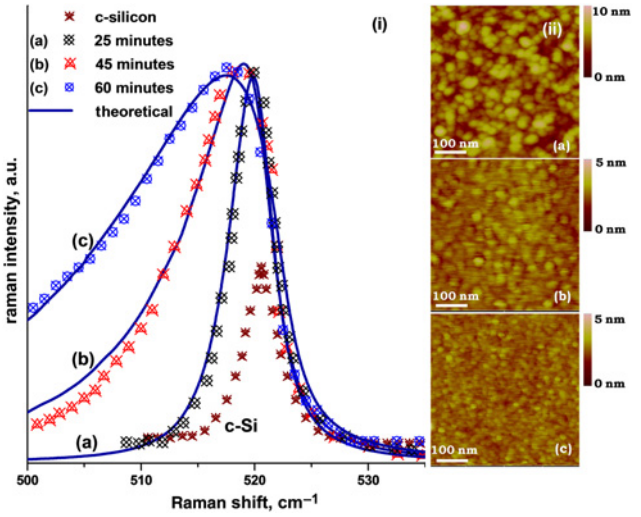

Figure 1 *(i) Comparison of experimental and theoretical Raman spectra of laser-etched sample*
Theoretically calculated Raman spectra using (1) are indicated by solid lines and the experimental data are plotted as discrete points. c-Si peak appears at 520.5 cm^{-1}
(*ii*) Two-dimensional AFM images of samples S1, S2 and S3 are shown in (a), (b) and (c), respectively

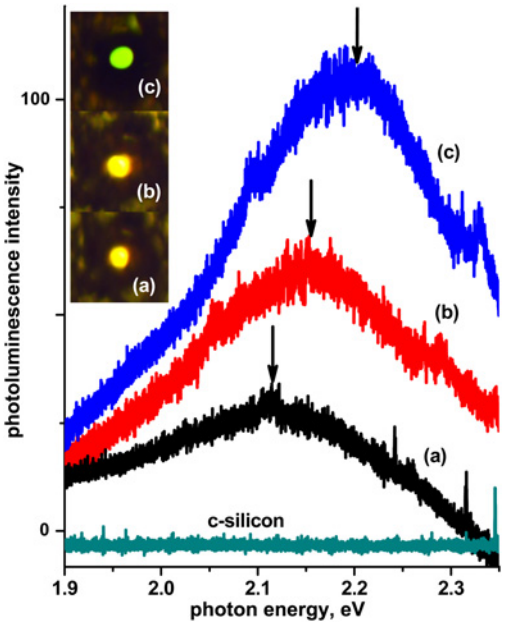

Figure 2 *Room-temperature PL spectra from samples S1, S2 and S3 are shown in (a), (b) and (c), respectively*
The inset of this figure shows the PL observed from Si NSs

Table 1 Calculated minimum, maximum and average sizes of samples S1, S2 and S3 calculated by fitting the Raman scattering data of these samples shown in Fig. 1

Samples	Theoretically calculated sizes		
	L_1, nm	L_2, nm	L_0, nm
S1	3.5	7.0	5.3
S2	3.0	5.8	4.5
S3	2.5	5.5	4.0

Figs.1(*ii*) (a)–(c) show two-dimensional atomic force microscope (AFM) images from samples S1, S2 and S3, respectively. Images shown in Fig. 1(*ii*) are high-resolution images taken from pore walls of the laser-etched samples. Fig. 1(*ii*) shows that the Si NSs have sizes in the range of a few nanometres. It is well known that the sizes of NSs seen in the AFM image are always greater than the sizes obtained by Raman data. This has been discussed by Wana *et al.* [19] because of the diameter of the AFM tip apex and the aspect ratio of sample and tip. However, both Raman data and AFM images show reduction of sizes with increased etching time.

PL spectra are studied here as a function of etching time. Figs. 2 (a)–(c) show the room-temperature PL spectra from samples S1, S2 and S3, respectively. The inset of Fig. 2 shows PL observed from Si NSs when it is viewed in the reflection by white light through a microscope assembly. Silicon normally emits only extremely weak infrared PL at low temperature because of its relatively small and indirect bandgap. Therefore PL is not observed for c-Si at room temperature as shown in Fig. 2. The PL from the sample S1 is shown in Fig. 2 (a), where a clear peak of about 2.11 eV is observed for in irradiation time of 25 min. With further increase in irradiation time to 45 min, the observed PL shows a clear hump about 2.16 eV in Fig 2 (b). As the irradiation time is further increased to 60 min, the observed PL shows a clear hump about 2.2 eV in Fig. 2 (c). Thus, a blue-shift in PL peak position is observed with increasing etching time.

Results reported in the literature indicate that visible PL in the range of 2.0–2.3 eV can be because of the quantum confinement of electrons in the Si NSs or because of defects at the interface of the nanoparticles/matrix or in the SiO_2 matrix itself [20, 21]. However, the LIE process has involvement of fluorine or hydrogen. Species such as SiF_4, $SiHF_4$ or H_2SiF_6, can form a passivation layer over the surface. It may generate recombination centres for the electrons, where PL is due to chemisorbed molecules over the surface [22]. Thus, a different radiative process is possible because of molecular agents and the PL band can be associated with molecules chemisorbed to the surface area of the NSs. In addition to this, the formation of oxide over the surface also can be the source of PL. Thus, it is important to exclude the effect of chemical species which may diminish the sole contribution of quantum confinement in the observed PL. In our case, the nanosized texture is itself on the Si surface. Therefore PL from NSs is not affected by the surrounding matrix and interfaces. To exclude the effect of chemical species and oxides, the samples were rinsed with hot water and ethanol to remove the species absorbed on the surface of NSs. A possible origin of visible PL is the quantum confinement of electrons since NSs are grown in isolation. Therefore size-dependent blue-shift of the PL peak position is attributed to the quantum confinement of electrons in LIE-generated Si NSs.

The size and size distribution of Si NSs, which may contribute efficiently to visible PL, are estimated here using the quantum confinement model proposed by Yorikawa and Muramatsu [23] They assume that each particle has a very sharp PL intensity for the ensemble of particles having Gaussian distribution $D(R_E)$ of sizes. The PL spectrum $S(E)$ is written as [23]

$$S(E) = C\alpha(E_{\text{exc}} - E)D(R_E)\frac{1}{\beta}\frac{R_E}{E - E_g^0} \tag{2}$$

where R_E is defined by $R_E = d = \left[\gamma/\left(E - E_g^0\right)\right]^{1/\beta}$. R_E represents the size of crystallites, which can emit photons with an energy E. $\gamma = 3.73$ (eV nm^{β}), $\beta = 0.9$ and Gaussian distribution $D(R_E) = \left(1/\sigma\sqrt{2\pi}\right)\exp\left[\left(R_E - R_0\right)/2\sigma\right]^2$ (where R_0 is the mean size of NSs) are utilised to fit our experimental PL data. Mean sizes of samples (S1, S2 and S3) calculated by (2) are shown by solid circles in Fig. 3. The inset of Fig. 3 shows the lineshape fitting of sample S3 using (2). There is a slight mismatch

doi: 10.1049/mnl.2012.0910

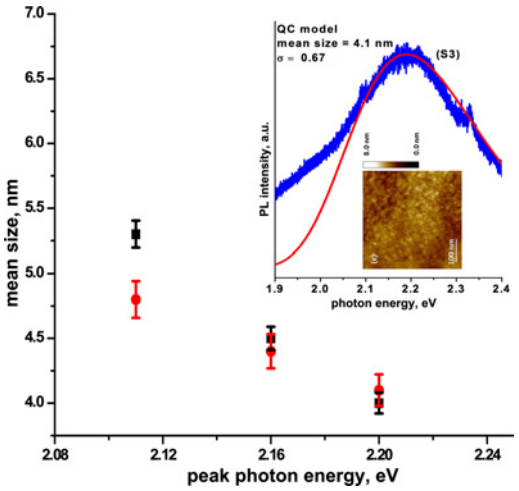

Figure 3 *Mean sizes calculated by (1) and (2) are shown by solid squares and solid circles, respectively*
Lineshape PL fitting using (2) and AFM image are shown in the inset for sample S3

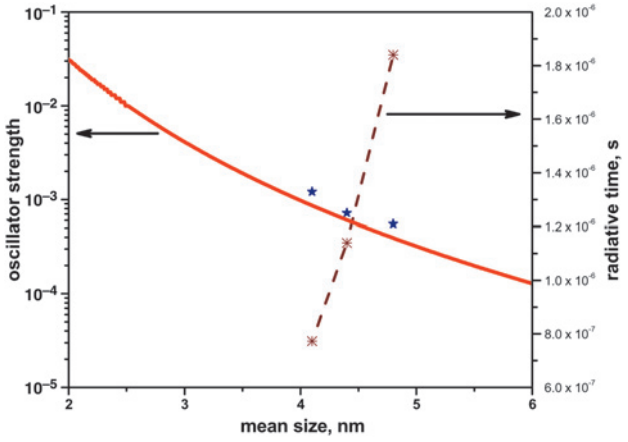

Figure 4 *Oscillator strength, f_{osc}, and radiative time τ_R plotted against particles size*
Solid star shows the f_{osc} calculated using PL spectra of samples S1, S2 and S3

between experimental and theoretical results towards the low energy side. This is attributed to the presence of a relatively less number of smaller size NSs over the laser-etched surface. Quantum confinement of optical phonons has been observed in Raman scattering of LIE-generated Si NSs. Mean sizes of Si NSs for samples (S1, S2 and S3) calculated by (1) are also shown by solid squares in Fig. 3. These sizes calculated using (1) and (2) lie in the range of 4–5.3 nm. Both results are in good agreement with each other. Therefore it is concluded that PL in the range of 1.9–2.3 eV is due to the quantum confinement of electrons and phonons in LIE-generated Si NSs.

Radiative lifetime is discussed here to rule out the PL because of defects. The size-dependent blue-shift of PL peak position is attributed to the quantum confinement effect. Significant increase in PL intensity is observed in Fig. 2 with the decrease in size of Si NSs. Therefore quantum efficiency of radiative transition [24] is increased with decreasing size of Si NSs. This attributes to the transition from indirect to direct recombination process that causes increase in oscillator strength (f_{osc}) and reduction of the radiative lifetime (τ_R) of electrons [24, 25]. Theoretically, the radiative recombination rate $R_R = \tau_R^{-1}$ is linked to the dipole-allowed optical transition matrix element $\left|\langle\psi_i|\hat{\boldsymbol{p}}|\rangle\psi_f\right|^2$ and the recombination frequency ω via Fermi's Golden rule. It is usually given by $\tau_R^{-1} = R_R = \left(e^2 n\omega/\pi\varepsilon_0 m^2 hc^3\right)\left|\langle\psi_i|\hat{\boldsymbol{p}}|\rangle\psi_f\right|^2$. The oscillator strength [26] of optical transition can be expressed as $f_{osc}(\omega) = (2/hm\omega)\left|\langle\psi_i|\hat{\boldsymbol{p}}|\rangle\psi_f\right|^2$. Therefore lifetime τ_R for dipole-allowed optical transitions can be calculated by the following simplified equation

$$\tau_R = \frac{2\pi\varepsilon_0 mc^3}{e^2 n\omega^2}\frac{1}{f_{osc}(\omega)} \tag{3}$$

where n is the refractive index of Si, c is the velocity of light and ω is the peak emission photon energy. The exciton mass m is the sum of m_e (~$0.19m_0$) and m_h (~$0.286m_0$), where m_0 is the rest mass of the electron. It is invoked that oscillator strength, f_{osc}, can be calculated by $f_{osc} \sim 4.3 \times 10^{-9} A$. A is the area under the PL spectrum for a given size in Fig. 2 when PL is measured in absolute wavenumber. f_{osc} calculated from our PL spectra and its dependence as d^{-5} proposed by Sanders and Chang [27] is plotted in Fig. 4. Both f_{osc} shown in Fig. 4 are in good agreement. τ_R, which is calculated by (3), is also plotted with particle size 'd' of LIE-generated Si NSs in Fig. 4. As size of the LIE-generated Si NSs is decreased, radiative lifetime is also decreased with increase of the quantum effect as shown in Fig. 4. The radiative lifetime shown in Fig. 4 suggests that the PL is not because of the defect-related effects which exhibit large decay rates. The calculated results are in close agreement with the experimentally predicted radiative lifetime for Si NSs [25]. Thus, the observed PL from LIE-generated Si NSs is solely because of the quantum confinement effect.

4. Conclusions: In summary, the PL forming Si NSs in the present work is explained in terms of the quantum confinement of electrons. The effect of matrix interface and other possible contributions in visible PL have been neglected by fabricating the Si NSs on the Si wafer itself. Blue-shift of the PL peak position on decreasing the size of Si NSs is attributed solely to the quantum confinement of electrons. Quantum confinement models have been used here to calculate the mean size of Si NSs using Raman and PL lineshape fitting. Good agreement between experimental results and theoretical calculations reveals the presence of the quantum confinement effect in Si NSs. Oscillator strength has been calculated by area under the PL curve, which shows good agreement with the size-dependent relation. Calculated radiative lifetime reveals the presence of radiative recombination in the quantum confined Si NSs.

5. Acknowledgments: The authors acknowledge financial support from the Department of Science and Technology, Government of India under the project 'Linear and non-linear optical properties of semiconductor/metal nanoparticles for optical/electronic devices'. V. Kumar acknowledges financial support from the University Grants Commission (UGC), India.

6 References

[1] Weiss S.M., Fauchet P.M.: 'Porous silicon one-dimensional photonic crystals for optical signal modulation', *IEEE J. Sel. Top. Quantum Electron.*, 2006, **12**, pp. 1514–1519
[2] Park J., Gu L., Maltzahn G., Ruoslahti E., Bhatia S.N., Sailor M.J.: 'Biodegradable luminescent porous silicon nanoparticles for in vivo applications', *Nature Mater.*, 2009, **8**, pp. 331–336
[3] Kerr M.J., Cuevas A.: 'General parameterization of Auger recombination in crystalline silicon', *J. Appl. Phys.*, 2002, **91**, pp. 2473–2480
[4] Schroder D.K.: 'Semiconductor material and device characterization' (Wiley-Interscience, Hoboken, Canada, 2006)

[5] Canham L.T.: 'Silicon quantum wire array fabrication by electrochemical and chemical dissolution of wafers', *Appl. Phys. Lett.*, 1990, **57**, pp. 1046–1048
[6] Hirschman K.D., Tsybeskov L., Duttagupta S.P., Fauchet P.M.: 'Silicon-based visible light-emitting devices integrated into microelectronic circuits', *Nature*, 1996, **384**, pp. 338–341
[7] Wilson W.L., Szajowski P.F., Brus L.E.: 'Quantum confinement in size-selected, surface-oxidized silicon nanocrystals', *Science*, 1993, **262**, pp. 1242–1244
[8] Lu Z.H., Lockwood D.J., Baribeau J.M.: 'Quantum confinement and light emission in SiO_2/Si superlattices', *Nature*, 1995, **378**, pp. 258–260
[9] Nassiopoulos A.G., Grigoropoulos S., Papadimitriou D.: 'Electroluminescent device based on silicon nanopillars', *Appl. Phys. Lett.*, 1996, **69**, pp. 2267–2269
[10] Tishler M.A., Collins R.T., Stathis J.H., Tsang J.C.: 'Luminescence degradation in porous silicon', *Appl. Phys. Lett.*, 1992, **60**, pp. 639–641
[11] Cullis A.G., Canham L.T.: 'Visible light emission due to quantum size effects in highly porous crystalline silicon', *Nature*, 1991, **353**, pp. 335–338
[12] Ray M., Bandyopadhyay N.R., Ghanta U., Klie R.F., Pramanick A. K.: 'Temperature dependent photoluminescence from porous silicon nanostructures: quantum confinement and oxide related transitions', *J. Appl. Phys.*, 2011, **110**, p. 094309
[13] Ding W., Zheng J., Qi W., Yu W., Fu G.: 'Dependence of the photoluminescence from silicon nanostructures on the size of silicon nanoparticles', *Proc. SPIE*, 2008, **7135**, p. 713508
[14] Estes M.J., Moddel G.: 'Luminescence from amorphous silicon nanostructures', *Phys. Rev. B*, 1996, **54**, pp. 14633–13642
[15] Kumar R., Mavi H.S., Shukla A.K.: 'Macro and microsurface morphology reconstructions during laser-induced etching of silicon', *Micron*, 2008, **39**, pp. 287–293
[16] Campbell I.H., Fauchet P.H.: 'The effects of microcrystal size and shape on the one phonon Raman spectra of crystalline semiconductors', *Solid State Commun.*, 1986, **58**, pp. 739–741
[17] Shukla A.K., Kumar V.: 'Low-frequency Raman scattering from silicon nanostructures', *J. Appl. Phys.*, 2011, **110**, p. 064317
[18] Mavi H.S., Shukla A.K., Kumar R., Rath S., Joshi B., Islam S.S.: 'Quantum confinement effects in silicon nanocrystals produced by laser-induced etching and CW laser annealing', *Semicond. Sci. Technol.*, 2006, **21**, pp. 1627–1632
[19] Wan Q., Wang T.H., Liu W.L., Lin C.L.: 'Ultra-high-density Ge quantumdots on insulator prepared by high-vacuum electron-beam evaporation', *J. Cryst. Growth*, 2003, **249**, pp. 23–27
[20] Maeda Y.: 'Visible photoluminescence from nanocrystallite Ge embedded in a glassy SiO_2 matrix: evidence in support of the quantum-confinement mechanism', *Phys. Rev. B*, 1995, **51**, pp. 1658–1670
[21] Wu X.M., Lu M.J., Yao W.G.: 'Structure and optical properties of SiO_2 films containing Ge nanocrystallites', *Surf. Coat. Technol.*, 2002, **161**, pp. 92–95
[22] Xu Z.Y., Gal M., Gross M.: 'Photoluminescence studies on porous silicon', *Appl. Phys. Lett.*, 1992, **60**, pp. 1375–1377
[23] Yorikawa H., Muramatsu S.: 'Logarithmic normal distribution of particle size from a luminescence line-shape analysis in porous silicon', *Appl. Phys. Lett.*, 1997, **71**, pp. 644–646
[24] Trwoga P.F., Kenyon A.J., Pitt C.W.: 'Modeling the contribution of quantum confinement to luminescence from silicon nanoclusters', *J. Appl. Phys.*, 1998, **83**, pp. 3789–3794
[25] Weissker H.-Ch., Furthmüller J., Bechstedt F.: 'Structure- and spin-dependent excitation energies and lifetimes of Si and Ge nanocrystals from ab initio calculations', *Phys. Rev. B*, 2004, **69**, p. 115310
[26] Henry C.: 'Lifetimes of bound excitons in CdS', *Phys. Rev. B*, 1970, **1**, pp. 1628–1634
[27] Sanders G.D., Chang Y.: 'Optical properties of free-standing silicon quantum wires', *Appl. Phys. Lett.*, 1992, **60**, pp. 2525–2527

doi: 10.1049/mnl.2012.0910